Coordinated Power Regulation of Clustered IBRs within Grid-Connected Local Energy Communities

Zaint A. Alexakis[a,*], Panos C. Papageorgiou[b], Antonio T. Alexandridis[b], Georgios Tzounas[c] and Charalambos Konstantinou[a]

[a] CEMSE Division, King Abdullah University of Science and Technology (KAUST), Thuwal, Saudi Arabia
[b] Department of Electrical and Computer Engineering, University of Patras, Patra, Greece
[c] School of Electrical and Electronic Engineering, University College Dublin, Dublin, D04V1W8, Ireland

ARTICLE INFO

Keywords:
Local energy communities (LECs)
Power sharing
Secondary control
Voltage source inverters (VSIs)
Stability analysis
Controller hardware-in-the-loop (CHIL)

ABSTRACT

Market-participating local energy communities (LECs) formed by aggregated inverter resources must satisfy their cleared bid quotas to avoid the monetary penalties imposed by balancing mechanisms. Although optimizers handle longer-timescale dispatch, these penalties persist because load and renewable energy source (RES)-generation volatility occurs on real-time scales that the optimizers cannot absorb, while conventional hierarchical control, which targets only frequency and voltage, does not regulate the aggregated LEC power. This paper proposes a novel power-coordination scheme for grid-connected LECs that regulates the combined output of the clustered converters while enforcing proportional active- and reactive-power allocation of the community quota. Building on the secondary-control structure, the scheme relies only on smart-meter measurements and low-bandwidth neighbor-to-neighbor communication among the coordinated units. The prescribed sharing is preserved even under stiff-grid conditions, where the connected resources cannot influence grid frequency or nodal voltages. The LEC objectives are likewise met regardless of the output of non-coordinated VSIs or load variability, without requiring any information about them. Owing to its simple structure, the scheme can be readily integrated into existing hierarchical and non-inverter control frameworks, reinforcing them with market-compliant LEC coordination. Stability and performance are validated through theoretical analysis, numerical simulations, and a CHIL benchmark.

1. Introduction

1.1. Motivation

Local energy communities (LECs) are distributed aggregations of flexible energy resources, such as electric vehicle chargers, solar photovoltaic systems, etc. [34, 15]. They promote participation of small-scale producers in energy markets [6, 12] and facilitate monitoring and management of distributed generation [13, 21]. They can also provide fast ancillary services that contribute to the stability and performance of the overall power system [37, 14]. A typical grid-connected LEC consists of clustered inverter-based resources (IBRs) connected in parallel at a point of common coupling (PCC). A LEC coordinates its generation resources in accordance with energy market and ancillary-service regulations, ensuring that its combined active and reactive power output tracks the contracted setpoints and thereby avoids real-time balancing penalties [9, 24, 32]. To this end, the aggregated commitments are dispatched proportionally among the community members in accordance with their rated capacities or other factors, ensuring uniform utilization of resources and preserving symmetric reserve margins for ancillary-service provision. Ensuring stable and timely power coordination among these VSIs, such that the LEC can reliably meet its market and ancillary obligations without incurring balancing penalties, is an emerging research challenge and the focus of this paper.

1.2. Literature Review

The coordination of grid-connected IBRs spans multiple time scales [28]. At longer time scales, load allocation is managed through steady-state active and reactive power set points, typically determined by solving an optimization

*Corresponding author
zaint.alexakis@kaust.edu.sa (Z.A. Alexakis); papageorgiou@ece.upatras.gr (P.C. Papageorgiou); a.t.alexandridis@ece.upatras.gr (A.T. Alexandridis); georgios.tzounas@ucd.ie (G. Tzounas); charalambos.konstantinou@kaust.edu.sa (C. Konstantinou)
ORCID(s):

problem [39, 29]. At shorter time scales, power imbalances between generation and demand during disturbances are compensated by automatically adjusting distributed energy resource (DER) power outputs through local controllers. To address the multi-time scale and multifaceted needs of power systems, engineers employ hierarchical control techniques. For example, primary-level controllers are often implemented as classical droop controllers for frequency and nodal voltage regulation, whereas load deviations are actively distributed among the controlled DERs [8, 17]. An important application of this framework is the control of microgrids. For example, [35, 36] use droop-based strategies to balance the state-of-charge among electric vehicles in a DC microgrid; in [19] droop control is employed to coordinate, through an adaptive virtual impedance, the reactive power sharing in an ac microgrid.

A key advantage of droop controllers is that they enable decentralized operation without requiring peer-to-peer communication [24]. This simplicity, however, comes at the cost of steady-state deviations in the frequency and voltage signals through which load power is allocated among DERs [17]. Such deviations are typically compensated by slower secondary-level controllers [38]. In this context, secondary control is employed for both voltage and frequency restoration: voltage-restoration loops adjust reactive-power references to recover prescribed voltage magnitudes, whereas frequency-restoration mechanisms, including automatic frequency restoration reserve (aFRR), adjust active-power references to recover the nominal system frequency after disturbances. Existing implementations range from centralized architectures, where supervisory signals coordinate local regulation actions [8], to decentralized schemes that rely on communication among neighboring units to achieve frequency and voltage restoration while preserving power sharing [18, 31, 33]. These paradigms involve different trade-offs in coordination, scalability, and communication requirements; although decentralized schemes have become prominent, centralized designs remain relevant, with data-driven methodologies continuing to address their systematic design and tuning [16]. Distributed secondary control is commonly formulated through multi-agent systems theory and can take different forms depending on the application [31]. In [10], the authors propose a predefined-time secondary controller for voltage restoration and current sharing in DC microgrids, with the objective of enhancing overall system performance. A finite-time controller is developed in [27], exhibiting increased resilience to time delays. An important prerequisite for hierarchical control is the ability of the regulated DERs to actively influence the network's frequency and voltages. Otherwise, primary control is reduced to direct power control, which induces significant steady-state deviations, while secondary control becomes ineffective because frequency restoration is practically infeasible. These conditions typically arise under stiff-network operation, where, without proper coordination between smaller and larger power units, the implementation of secondary control becomes impractical.

Furthermore, with regard to the stability of hierarchical-control applications in power systems, this is usually assessed through time-domain simulations or small-signal analysis [7]. These are parameter-dependent approaches and thus, capturing in a comprehensive manner the relationship between stability and system parameters can become computationally cumbersome. As an alternative, analytical investigations through matrix theory can lead, under certain modeling assumptions, to useful insights about closed-loop stability. For instance, [25] presents an analytical stability investigation of a microgrid with resources equipped with both primary- and secondary-level controllers, using matrix theory. The analysis derives parameter-oriented stability conditions that ensure system stability without requiring eigenvalue calculations of the closed-loop system.

Although hierarchical control remains foundational to secure and coordinated grid operation, its primary objectives, namely frequency and voltage regulation, do not address the timely dispatch maneuvers required to comply with cleared market bids and avoid production-mismatch penalties. Market-driven coordination of clustered resources is instead conventionally performed at slower time-scales through centralized optimization routines that demand explicit knowledge of every coordinated unit. Representative formulations are reported in [20], where a centralized optimizer determines the operating setpoints of clustered resources, and in analogous schemes targeting aggregators and energy communities [2, 11]. The defining limitations of such approaches are twofold: they rely on information-intensive centralized coordination, requiring detailed unit-level measurements, capability data, and explicit setpoint allocation, while remaining poorly suited to absorb fast load and generation volatility at operational time scales, which can produce aggregate power mismatches that trigger balancing penalties and corrective redispatch or curtailment. Although real-time implementations have been reported [5], their centralized information processing and direct resource-level setpoint allocation constitute real-time dispatch rather than closed-loop decentralized coordination, leaving open the need for approaches that more seamlessly bridge market-level dispatch and device-level regulation. This work bridges this gap by proposing a distributed coordination scheme that operates at inverter time-scales to reinforce these market-level algorithms, drawing solely on the aggregate measurement at the PCC and remaining effective without any information

Table 1
Comparison of LEC coordination paradigms across capabilities relevant to LEC operation.

Coordination paradigm	**C1**	**C2**	**C3**	**C4**	**C5**
Standalone primary level control [17, 40, 1]	✗	✓	✓	∘	✗
Hierarchical with centralized secondary [8, 16]	✗	✗	✓	∘	∘
Hierarchical with decentralized secondary [18, 31, 33, 10, 27]	✗	✓	✓	✓	∘
Centralized dispatch/optimization-based coordination [5, 2, 11]	✓	✗	✗	✗	✓
Proposed scheme	✓	✓	✓	✓	✓

C1: ability to coordinate the aggregate power output of the energy community at the PCC. **C2**: operates without requiring explicit information from every participating unit. **C3**: ability to provide grid-supporting services. **C4**: provides analytical large-signal stability conditions. **C5**: compliant with energy-market dispatch requirements. ✓: capability satisfied; ∘: partially or conditionally satisfied; ✗: not satisfied.

about non-coordinated resources operating under autonomous policies. Table 1 summarizes how the proposed scheme compares against the closest existing coordination paradigms across the capabilities relevant to LEC operation.

1.3. Contribution

Given the limitations of existing techniques identified in the literature, this paper proposes a novel control framework to regulate grid-connected IBRs within LEC frameworks. The objective is to manage the cluster's power output while proportionally distributing the power quotas among the community's coordinated converters. Building on the conventional secondary-control structure, the controller leverages a low-bandwidth communication network and readily available smart meter measurements to regulate the LEC power output. Although the proposed scheme is designed based on a direct power-control grid following (GFL) architecture, it can be readily adapted to other inverter and non-inverter control frameworks, including hierarchical control schemes, reinforcing them with the ability to regulate LECs at inverter time-scales with respect to energy market obligations. Analytical stability results are derived that remain valid even under partial participation of the LEC members, load variations, or imprecise knowledge of the VSI filter inductances. The proposed design remains effective under severe LEC load variability, power fluctuations from non-coordinated converters, and stiff-grid operation, where the connected resources cannot appreciably influence the grid frequency. Numerical simulations and controller hardware-in-the-loop (CHIL) experiments on a representative LEC under non-ideal conditions validate these results and demonstrate the controller's performance.

1.4. Organization

The remainder of the paper is organized as follows. Section 2 describes the LEC modeling. The proposed power sharing control scheme is presented in Section 3. Simulation results are discussed in the case study provided in Section 4, while experimental results are presented in Section 5. Finally, conclusions are presented in Section 6.

2. Energy Community Modeling

We consider a grid-connected LEC consisting of N inverter-based DER units. The DER units supply their individual complex loads, $\left(P_{l,i}, Q_{l,i}\right)$, and are connected in parallel at a PCC, which is the LEC connection point to the main power grid. An illustrative description of the considered LEC modeling is depicted in Fig. 1. This setup represents the majority of LECs found in the distribution network, where end-users are connected in parallel to the distribution feeder [40]. For our analysis, we consider the voltage source equivalent model of a VSI, which consists of a three-phase voltage source connected to a RL filter. Every VSI is supplied by its respective DER unit, modeled for our needs as a constant DC voltage source $v_{\mathrm{dc},i}$. Considering a synchronously rotating dq-frame, the i-th VSI output current is:

$$l_i \iota'_{d,i} = -r_i \iota_{d,i} + \omega_{\mathrm{ac},i} l_i \iota_{q,i} + m_{d,i} v_{\mathrm{dc},i} - v_{\mathrm{ac},d,i}, \tag{1}$$

$$l_i \iota'_{q,i} = -r_i \iota_{q,i} - \omega_{\mathrm{ac},i} l_i \iota_{d,i} + m_{q,i} v_{\mathrm{dc},i} - v_{\mathrm{ac},q,i}, \tag{2}$$

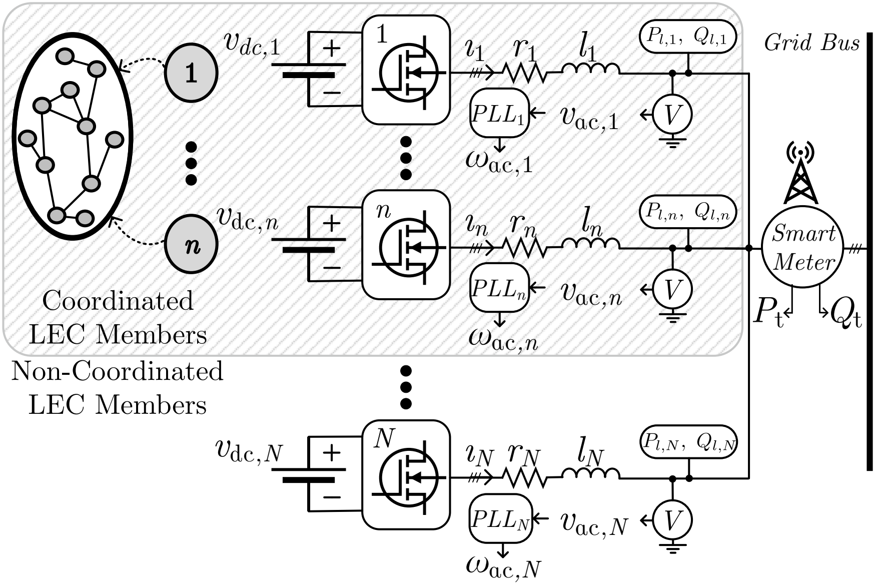

Figure 1: Physical and communication layers of LEC.

where $i \in \mathbb{S}$, with $\mathbb{S} = 1, 2, \ldots, N$; l_i, r_i are the aggregated inductance and resistance, respectively, of the VSI filter and of the line connecting the VSI to the PCC; $\imath_{d,i}$, $\imath_{q,i}$ are the d- and q-axis components of the VSI current $\imath_i$, with $\imath_i^2 = \imath_{d,i}^2 + \imath_{q,i}^2$; $m_{d,i}$, $m_{q,i}$ denote the VSI Park-transformed duty ratios; in line with GFL operation, $\omega_{\mathrm{ac},i}$ is the frequency of the inverter's rotating frame and is obtained through a phase-locked loop (PLL); and $v_{\mathrm{ac},d,i}$, $v_{\mathrm{ac},q,i}$ are the d- and q-axis components of the ac-side voltage, $v_{\mathrm{ac},i}$. We note that in the considered formulation, each VSI has a distinct dq frame and thus the AC-side voltages in (1)-(2) are denoted with index i. The active and reactive power output of the i-th VSI are given by:

$$\begin{aligned} P_i &= 1.5 \cdot \left(v_{\mathrm{ac},d,i}\imath_{d,i} + v_{\mathrm{ac},q,i}\imath_{q,i} \right), \\ Q_i &= 1.5 \cdot \left(v_{\mathrm{ac},q,i}\imath_{d,i} - v_{\mathrm{ac},d,i}\imath_{q,i} \right). \end{aligned} \tag{3}$$

The main objective of the grid-connected LEC is to regulate its active power output P_{t} and reactive power output Q_{t} at the PCC, where:

$$P_{\mathrm{t}} = \sum_{i=1}^{N} P_i - P_{l,i}, \quad Q_{\mathrm{t}} = \sum_{i=1}^{N} Q_i - Q_{l,i}$$

Achieving this objective requires proper coordination of the VSIs comprising the LEC. In this work, such a coordination is achieved through a proportional allocation of power quotas, as follows:

$$\begin{aligned} k_{P,i}P_i^* &= k_{P,j}P_j^*, \quad k_{Q,i}Q_i^* = k_{Q,j}Q_j^*, \quad i, j \in \mathbb{S}_{\mathbb{P}} \\ P_{\mathrm{t}}^{\mathrm{ref}} &= \sum_{i\in\mathbb{S}} \left(P_i^* - P_{l,i}\right), \quad Q_{\mathrm{t}}^{\mathrm{ref}} = \sum_{i\in\mathbb{S}} \left(Q_i^* - Q_{l,i}\right), \end{aligned} \tag{4}$$

where $k_{P,i}, k_{Q,i}, P_i^*, Q_i^*$ denote the i-th VSI droop gains and steady-state active and reactive power outputs, respectively; with $\mathbb{S}_{\mathbb{P}} \subseteq \mathbb{S}$ we denote the subset of VSIs that participate in power sharing; correspondingly, we will denote with $\mathbb{S}_{\mathbb{NP}} \subseteq \mathbb{S}$ the remaining VSIs that do not participate in power sharing, so that $\mathbb{S} = \mathbb{S}_{\mathbb{P}} \cup \mathbb{S}_{\mathbb{NP}}$. That is, not all community members need to be dispatched to fulfill the objective described in (4), and the LEC operator must be able to effectively compensate the active and reactive power injections of the non-participating units, as well as the volatility of connected loads. In addition, the LEC active and reactive power set points, $P_{\mathrm{t}}^{\mathrm{ref}}$ and $Q_{\mathrm{t}}^{\mathrm{ref}}$, are assumed to be bounded constants determined by the LEC operator. Their values depend on the activities of the LEC, such as energy market participation, power purchase agreements, or net-zero targets.

The LEC active and reactive power outputs P_t and Q_t are measured through a smart meter connected at the terminal point with the main grid. The smart meter acts as a central unit that, through a unidirectional communication link, provides to the IBRs participating in power sharing the errors between the set point and actual power output of the LEC:

$$\epsilon_P = P_\mathrm{t}^\mathrm{ref} - P_\mathrm{t}, \quad \epsilon_Q = Q_\mathrm{t}^\mathrm{ref} - Q_\mathrm{t}. \tag{5}$$

The overall power output per se, as well as the power generation and consumption of individual LEC members remain classified, thus ensuring that their anonymity and privacy are preserved. Furthermore, DERs participating in the power sharing scheme are assumed to have the ability to communicate their power outputs with adjacent DERs. This is achieved through a bidirectional, low-bandwidth neighbor-to-neighbor communication network, represented by a connected and unweighted graph. This graph is denoted as $G(\mathbb{V}, \mathbb{E}, \boldsymbol{\mathcal{A}})$, where $\mathbb{V}$ is the set of vertices, representing DERs; and $\mathbb{E}$ is the set of edges, representing the communication links between DERs. The Laplacian matrix of the graph $\boldsymbol{\mathcal{L}} \in \mathbb{R}^{n\times n}$ is defined as $\boldsymbol{\mathcal{L}} = \mathrm{diag}\left(\boldsymbol{\mathcal{A}}\mathbf{1}_n\right) - \boldsymbol{\mathcal{A}}$, where $\mathbf{1}_n$ denotes a column vector of ones of size n, $\mathbf{1}_n = [1 \dots 1]^\mathsf{T}$; and $\boldsymbol{\mathcal{A}}$ denotes the adjacency matrix. We note that the fact that the communication network graph is connected implies that the algebraic multiplicity of the zero eigenvalue of $\boldsymbol{\mathcal{L}}$ is equal to one.

3. Controller for LEC Coordination

As primary and secondary controllers regulate frequency and nodal voltages, they cannot address the objectives of the LEC presented in (4), especially under stiff-grid conditions. Recognizing this limitation and leveraging the control structure of secondary controllers along with available LECs' resources, such as smart meter measurements, we propose a novel control structure in this section to effectively satisfy the community objectives.

3.1. Proposed Control Scheme

The proposed controller is illustrated in Fig. 2. It consists of two loops, corresponding to the $d-$ and $q-$ axis duty ratio components of the i-th VSI. Each loop primarily comprises an integral term employed to satisfy the LEC objectives described in (4), and a proportional term that enhances the LEC transient performance. In line with direct power GFL control architectures, the proposed control structure directly regulates the active and reactive power of the LEC in a single stage. The controller is incorporated in the inner VSI control loops of the $n < N$ community members coordinated by the LEC operator. The active and reactive power outputs of these n community members are denoted as $P_s = \sum_{i\in\mathbb{S}_\mathbb{P}} P_i$ and $Q_s = \sum_{i\in\mathbb{S}_\mathbb{P}} Q_i$, respectively, where $\mathbb{S}_\mathbb{P} = \{i \in \mathbb{S} \mid 1 \le i \le n\}$. The remaining $N - n$ members are operating independently, with their active and reactive power outputs being denoted as $P_{ns} = \sum_{i\in\mathbb{S}_\mathbb{NP}} P_i$ and $Q_{ns} = \sum_{i\in\mathbb{S}_\mathbb{NP}} Q_i$, respectively, where $\mathbb{S}_\mathbb{NP} = \{i \in \mathbb{S} \mid n+1 \le i \le N\}$.

The duty ratio components $m_{d,i}$ and $m_{q,i}$ are defined as follows:

$$m_{d,i} = v_{\mathrm{dc},i}^{-1}(-k_{pd,i}\imath_{d,i} - \omega_{\mathrm{ac},i}l_{\mathrm{est},i}\imath_{q,i} + k_{zd,i}z_{d,i} + v_{\mathrm{ac},d,i}), \tag{6}$$

$$m_{q,i} = v_{\mathrm{dc},i}^{-1}(-k_{pq,i}\imath_{q,i} + \omega_{\mathrm{ac},i}l_{\mathrm{est},i}\imath_{d,i} + k_{zq,i}z_{q,i} + v_{\mathrm{ac},q,i}), \tag{7}$$

where $k_{pd,i}$, $k_{pq,i}$, $k_{zd,i}$, $k_{zq,i}$ are the droop coefficients of the sharing scheme; and $l_{\mathrm{est},i}$ is the estimated VSI inductance used to decouple the current into its d and q components.

We note that, in industrial applications, the estimated VSI filter inductance $l_{\mathrm{est},i}$ often differs from its actual value l_i. This leads to an error $l_{\epsilon,i} = l_i - l_{\mathrm{est},i} \neq 0$ and, hence, to an inexact decoupling of the current. In this work, inexact decoupling is duly taken into account in the formulation of the proposed control as well as in the stability analysis conducted in Section 3.3.

The dynamics of the integrator states $z_{d,i}$ and $z_{q,i}$ are defined as follows:

$$z'_{d,i} = \epsilon_P - k_{P,i} \sum_{j\in\Omega_i} a_{ij}\left(k_{P,i}P_i - k_{P,j}P_j\right) \tag{8}$$

$$z'_{q,i} = -\epsilon_Q + k_{Q,i} \sum_{j\in\Omega_i} a_{ij}\left(k_{Q,i}Q_i - k_{Q,j}Q_j\right) \tag{9}$$

where a_{ij} are the elements of the communication network Laplacian matrix $\boldsymbol{\mathcal{L}}$; Ω_i corresponds to the neighborhood set of the i-th node of the communication network. Note that the simple structure of (8) and (9) enables the regulation

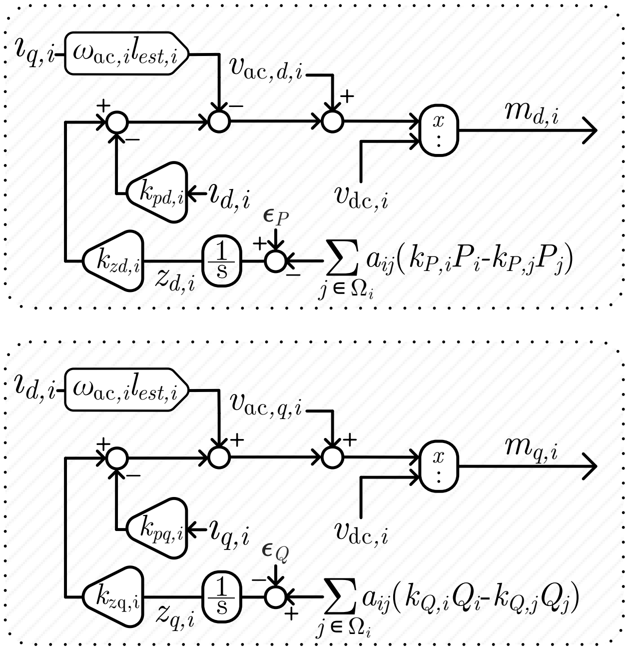

Figure 2: Control system diagram.

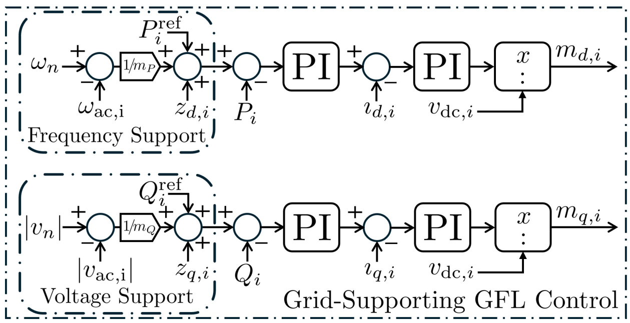

Figure 3: Embedding LEC coordination into grid-supporting GFL control.

of the errors ϵ_P and ϵ_Q as well as of the terms $\sum_{j\in\Omega_i} a_{ij}\left(k_{P,i}P_i - k_{P,j}P_j\right)$ and $\sum_{j\in\Omega_i} a_{ij}\left(k_{Q,i}Q_i - k_{Q,j}Q_j\right)$ to zero. A more in-depth investigation of how this property impacts the steady state and the satisfaction of (4) is provided in Section 3.2.

The selection and tuning of the controller gains is straightforward, owing to the developed models and the simple structure of the proposed scheme. The ratios between the gains $k_{P,i}$, and similarly between the $k_{Q,i}$, determine the power allocation quotas among the coordinated units; their values must therefore be chosen in accordance with the rated power of each member or, alternatively, through an optimization process. The absolute magnitudes of these gains, in turn, govern the strength of the proportional-sharing terms in (8) and (9): for the same ratios, larger magnitudes weight the sharing term more heavily than the aggregate-tracking error, leading the controller to enforce proportional sharing first and regulate the aggregate output thereafter, whereas smaller magnitudes invert this priority. The coefficient matrices $\mathbf{K}_{zd}$ and $\mathbf{K}_{zq}$ play an analogous role, governing the convergence rate of the integrator states in the same manner as the integral gain of a conventional PI controller. Finally, the matrices $\mathbf{K}_{pd}$ and $\mathbf{K}_{pq}$ set the level of damping in the current dynamics; larger values slow the response while suppressing oscillations, and must therefore be tuned in coordination with $\mathbf{K}_{zd}$ and $\mathbf{K}_{zq}$, in the same fashion as the proportional gain in conventional current control.

Observing the controllers structure, we make the following remark.

Remark 1. *Although the proposed framework is developed for the direct power control structure of* (6)–(9)*, it is not restricted to this architecture. The coordination layer can be readily integrated into conventional hierarchical control architectures while preserving their objectives, and it extends to non-inverter resources such as diesel generators or microturbines, since it relies only on the measured power outputs P_i, Q_i and the communication-graph connectivity, which remain accessible regardless of how each unit is realized.*

The integration of the proposed coordination layer into a conventional grid-supporting hierarchy is illustrated in Fig. 3. In this arrangement, the coordination layer provides a supervisory interface between community-level dispatch objectives and local converter controllers. By generating power references consistent with market dispatch and ancillary-service requirements, it complements the primary droop mechanisms and secondary restoration loops without altering their internal operation. Notably, the secondary controller need only determine the aggregate power adjustment required at the community level, which the proposed coordination layer then allocates among participating resources through the local power references. As a result, individual converters require neither independent secondary-control functionality nor direct communication links with external actors, reducing both coordination complexity and communication requirements while preserving frequency and voltage support capabilities. Overall, grid-supporting functionality and LEC-level coordination coexist within a unified control architecture that enables real-time regulation of aggregate community power. This is further illustrated in Section 4.

The selection of the reference setpoints $P_{\mathrm{t}}^{\mathrm{ref}}$ and $Q_{\mathrm{t}}^{\mathrm{ref}}$ is intrinsically tied to the operational posture of the LEC. When the aggregator engages strategically in energy markets (day-ahead, intra-day, or flexibility platforms), these references emerge from tertiary-layer optimization that internalizes economic objectives through profit maximization. Conversely, when the aggregator assumes an active role in ancillary-service provision, offering, for instance, aFRR, the reference generation may be entrusted to conventional secondary-control mechanisms, realized either via direct integral regulation of the frequency or through decentralized formulations such as the distributed-averaging proportional-integral (DAPI) controller [31].

Building upon this coordination layer, the following analysis adopts a set of standard steady-state and time-scale separation assumptions that enable a tractable representation of the underlying converter dynamics. Specifically, as the PLL dynamics converge considerably faster than the controller ones, we first assume that $\omega_{\mathrm{ac},i} = \omega$, where ω denotes the grid-bus frequency tracked by the PLL [3]; and second, that $\upsilon_{\mathrm{ac},d,i}$ is equal to the grid rms voltage υ_{ac}, since $\upsilon_{\mathrm{ac},q,i}$ is then practically zero. Under these assumptions, (3) simplifies to:

$$
\begin{aligned}
P_i &= c\ \iota_{d,i},\\
Q_i &= -c\ \iota_{q,i},
\end{aligned}
\tag{10}
$$

where $c = 1.5\upsilon_{\mathrm{ac}}$. Using (10), and incorporating (6)-(9) in (1) and (2), the closed-loop setting is:

$$l_i\iota'_{d,i} = -\left(r_i + k_{pd,i}\right)\iota_{d,i} + \omega l_{\epsilon,i}\iota_{q,i} + k_{zd,i}z_{d,i}, \tag{11}$$

$$l_i\iota'_{q,i} = -\left(r_i + k_{pq,i}\right)\iota_{q,i} - \omega l_{\epsilon,i}\iota_{d,i} + k_{zq,i}z_{q,i}, \tag{12}$$

where $i \in \mathbb{S}_{\mathbb{P}}$.

In the system described by (8), (9), (11), (12), the active and reactive power injections of the $N-n$ non coordinated members can be considered as bounded external inputs [4]. Using (5) and (10), we define:

$$P_{\mathrm{u}} = P_{\mathrm{t}}^{\mathrm{ref}} + \sum_{i\in\mathbb{S}} P_{l,i} - \sum_{i=n+1}^{N} c\iota_{d,i}, \tag{13}$$

$$Q_{\mathrm{u}} = -Q_{\mathrm{t}}^{\mathrm{ref}} - \sum_{i\in\mathbb{S}} Q_{l,i} - \sum_{i=n+1}^{N} c\iota_{q,i}, \tag{14}$$

Finally, the LEC equivalent model with inclusion of the proposed LEC coordination scheme can be written in the following matrix form:

$$\boldsymbol{L}\boldsymbol{\iota}'_d = -(\boldsymbol{R} + \mathbf{K}_{pd})\boldsymbol{\iota}_d + \omega\boldsymbol{L}_\epsilon\boldsymbol{\iota}_q + \mathbf{K}_{zd}\boldsymbol{z}_d, \tag{15}$$

$$\boldsymbol{L}\boldsymbol{\iota}'_q = -(\boldsymbol{R} + \mathbf{K}_{pq})\boldsymbol{\iota}_q - \omega\boldsymbol{L}_\epsilon\boldsymbol{\iota}_d + \mathbf{K}_{zq}\boldsymbol{z}_q, \tag{16}$$

where

$$
\begin{aligned}
&\boldsymbol{\iota}_d = \left[\iota_{d,1}, \dots, \iota_{d,n}\right]^\intercal,\ \boldsymbol{\iota}_q = \left[\iota_{q,1}, \dots, \iota_{q,n}\right]^\intercal,\\
&\boldsymbol{z}_d = \left[z_{d,1}, \dots, z_{d,n}\right]^\intercal,\ \boldsymbol{z}_q = \left[z_{q,1}, \dots, z_{q,n}\right]^\intercal,\\
&\mathbf{K}_{zd} = \mathrm{diag}(k_{zd,1}, \dots, k_{zd,n}),\ \mathbf{K}_{zq} = \mathrm{diag}(k_{zq,1}, \dots, k_{zq,n}),\\
&\mathbf{K}_{pd} = \mathrm{diag}(k_{pd,1}, \dots, k_{pd,n}),\ \mathbf{K}_{pq} = \mathrm{diag}(k_{pq,1}, \dots, k_{pq,n}),\\
&\boldsymbol{R} = \mathrm{diag}(r_1, \dots, r_n),\ \boldsymbol{L} = \mathrm{diag}(l_1, \dots, l_n),\\
&\boldsymbol{L}_\epsilon = \mathrm{diag}(l_{\epsilon,1}, \dots, l_{\epsilon,n}).
\end{aligned}
$$

To complete the compact representation, the integrator equations (8) and (9) are stacked over the n coordinated members, the aggregate-error terms, stacked as $\epsilon_P \mathbf{1}_n$ and $\epsilon_Q \mathbf{1}_n$, reduce through (13) and (14) to $\mathbf{1}_n P_\mathrm{u} - \mathbf{1}_{n\times n}\boldsymbol{P}$ and $\mathbf{1}_n Q_\mathrm{u} - \mathbf{1}_{n\times n}\boldsymbol{Q}$, respectively, while the proportional-sharing sums $k_{P,i}\sum_{j\in\Omega_i} a_{ij}\left(k_{P,i}P_i - k_{P,j}P_j\right)$ and their reactive counterparts assemble into the Laplacian terms $\mathbf{K}_P\boldsymbol{\mathcal{L}}\mathbf{K}_P\boldsymbol{P}$ and $\mathbf{K}_Q\boldsymbol{\mathcal{L}}\mathbf{K}_Q\boldsymbol{Q}$. Substituting $\boldsymbol{P} = c\boldsymbol{\iota}_d$ and $\boldsymbol{Q} = -c\boldsymbol{\iota}_q$ from (10), the integrator dynamics become:

$$\boldsymbol{z}_d' = -c\left(\mathbf{1}_{n\times n} + \mathbf{K}_P\boldsymbol{\mathcal{L}}\mathbf{K}_P\right)\boldsymbol{\iota}_d + \mathbf{1}_n P_\mathrm{u}, \tag{17}$$

$$\boldsymbol{z}_q' = -c\left(\mathbf{1}_{n\times n} + \mathbf{K}_Q\boldsymbol{\mathcal{L}}\mathbf{K}_Q\right)\boldsymbol{\iota}_q + \mathbf{1}_n Q_\mathrm{u}, \tag{18}$$

where $\mathbf{1}_{n\times n} = \mathbf{1}_n\mathbf{1}_n^\intercal$ and

$$\mathbf{K}_P = \mathrm{diag}(k_{P,1}, \dots, k_{P,n}),\ \mathbf{K}_Q = \mathrm{diag}(k_{Q,1}, \dots, k_{Q,n}).$$

3.2. Steady State

In this section, we show that the proposed control satisfies (4) in steady state. We start by considering (17) in steady state, where $\boldsymbol{z}_d' = \mathbf{0}_{n\times 1}$, with the notation $\mathbf{0}_{n\times m}$ describing the $n \times m$ zero matrix. We have:

$$c\left(\mathbf{1}_{n\times n} + \mathbf{K}_P\boldsymbol{\mathcal{L}}\mathbf{K}_P\right)\boldsymbol{\iota}_d^* = \mathbf{1}_n P_\mathrm{u}^*, \tag{19}$$

where $\boldsymbol{\iota}_d^* = \left[\iota_{d,1}^*, \dots, \iota_{d,n}^*\right]^\intercal$, is the steady-state d-axis current vector and P_u^* is given by

$$P_\mathrm{u}^* = P_\mathrm{t}^\mathrm{ref} + \sum_{i\in\mathbb{S}} P_{l,i} - \sum_{i=n+1}^{N} c\iota_{d,i}^*. \tag{20}$$

Multiplying from the left by $\mathbf{K}_P^{-1}$ ($\mathbf{K}_P$ is full rank):

$$c\mathbf{K}_P^{-1}\mathbf{1}_{n\times n}\boldsymbol{\iota}_d^* + c\boldsymbol{\mathcal{L}}\mathbf{K}_P\boldsymbol{\iota}_d^* = \mathbf{K}_P^{-1}\mathbf{1}_n P_\mathrm{u}^*. \tag{21}$$

The above expression is multiplied by $\mathbf{1}_n^\intercal$ and considering that $\mathbf{1}_{n\times n} = \mathbf{1}_n\mathbf{1}_n^\intercal$ and $\mathbf{1}_n^\intercal\boldsymbol{\mathcal{L}} = \mathbf{0}_{1\times n}$:

$$c\mathbf{1}_n^\intercal\mathbf{K}_P^{-1}\mathbf{1}_n\mathbf{1}_n^\intercal\boldsymbol{\iota}_d^* = \mathbf{1}_n^\intercal\mathbf{K}_P^{-1}\mathbf{1}_n P_\mathrm{u}^*. \tag{22}$$

Noticing that $c\mathbf{1}_n^\intercal\mathbf{K}_P^{-1}\mathbf{1}_n = \sum_{i=1}^n k_{P,i}^{-1}$ and through simple algebraic manipulations, (22) can be decomposed into:

$$c\mathbf{1}_n^\intercal\boldsymbol{\iota}_d^* = P_\mathrm{u}^*. \tag{23}$$

Finally, substituting P_u^* from (20) yields:

$$\sum_{i=1}^{N} c\iota_{d,i}^* - \sum_{i\in\mathbb{S}} P_{l,i} = \sum_{i\in\mathbb{S}}\left(P_i^* - P_{l,i}\right) = P_\mathrm{t}^\mathrm{ref}. \tag{24}$$

Equation (24) confirms that the community members always regulate the active power sum to the reference value, regardless of the behavior of the non power-sharing VSIs.

To establish the proportional relation between the active powers of the coordinated members, (23) is left-multiplied with $\mathbf{1}_n$:

$$c\mathbf{1}_{n\times n}\boldsymbol{\imath}_d^* = \mathbf{1}_n P_\mathrm{u}^*. \tag{25}$$

Replacing (25) into (19) and multiplying from the left with $\mathbf{K}_P^{-1}$, we end up with:

$$\boldsymbol{\mathcal{L}}\mathbf{K}_P\, c\boldsymbol{\imath}_d^* = \mathbf{0}_{n\times 1}. \tag{26}$$

Since $\boldsymbol{\mathcal{L}}$ has a one-dimensional null space spanned by $\mathbf{1}_n$ [31], the above expression forces the vector $\mathbf{K}_P c\boldsymbol{\imath}_d^*$ to be a scalar multiple of $\mathbf{1}_n$. Consequently, all its entries take a common value, i.e., $k_{P,i}c\imath_{d,i}^* = k_{P,j}c\imath_{d,j}^*$, or equivalently through (10), $k_{P,i}P_i^* = k_{P,j}P_j^*$ for all $i, j \in \mathbb{S}_\mathbb{P}$, which establishes the desired proportional relation between the active power outputs of the coordinated VSIs, satisfying the first condition of (4).

For the sake of simplicity, we conduct this analysis only for the active power. Analogous results can be obtained for the reactive power following a similar approach. Note that in steady state, the controller satisfies (4) irrespective of the output of the $N - n$ non-coordinated units and the active and reactive power load variations. Also, it is remarkable that the proposed integrator states (8) and (9) can always satisfy the requisites of (4), regardless of the considered LEC model. That is the case, as a similar analysis to the one conducted in this section can be followed and establish the fulfillment of the LEC objectives.

3.3. Stability Analysis

In this section, we investigate the stability of (15)-(18). To this end, we exploit various symmetry and skew-symmetry properties of the matrices of the formulated LEC model. We start the analysis by defining the column vector $\boldsymbol{x} = [\boldsymbol{\imath}_d\ \boldsymbol{\imath}_q\ \boldsymbol{z}_d\ \boldsymbol{z}_q]^\intercal$, $\boldsymbol{x} \in \mathbb{R}^{4n}$, and rewrite (15)-(18) in the following equivalent form:

$$\boldsymbol{x}' = \boldsymbol{J}\boldsymbol{x} + \left[\begin{array}{c}\mathbf{0}_{n\times1}\\ \mathbf{0}_{n\times1}\\ \hline \mathbf{1}_n\\ \mathbf{0}_{n\times1}\end{array}\right]P_\mathrm{u} + \left[\begin{array}{c}\mathbf{0}_{n\times1}\\ \mathbf{0}_{n\times1}\\ \hline \mathbf{0}_{n\times1}\\ \mathbf{1}_n\end{array}\right]Q_\mathrm{u}, \tag{27}$$

with $\boldsymbol{J} = \begin{bmatrix}-\boldsymbol{J}_{11} & \boldsymbol{J}_{12}\\ -\boldsymbol{J}_{21} & \mathbf{0}_{2n\times2n}\end{bmatrix}$ and $\boldsymbol{J}_{11}$, $\boldsymbol{J}_{12}$, $\boldsymbol{J}_{21}$ given by:

$$\boldsymbol{J}_{11} = \begin{bmatrix}\boldsymbol{L}^{-1}(\boldsymbol{R}+\mathbf{K}_{pd}) & \omega\boldsymbol{L}^{-1}\boldsymbol{L}_\epsilon\\ -\omega\boldsymbol{L}^{-1}\boldsymbol{L}_\epsilon & \boldsymbol{L}^{-1}(\boldsymbol{R}+\mathbf{K}_{pq})\end{bmatrix},$$
$$\boldsymbol{J}_{12} = \begin{bmatrix}\boldsymbol{L}^{-1}\mathbf{K}_{zd} & \mathbf{0}_{n\times n}\\ \mathbf{0}_{n\times n} & \boldsymbol{L}^{-1}\mathbf{K}_{zq}\end{bmatrix},$$
$$\boldsymbol{J}_{21} = \begin{bmatrix}c\left(\mathbf{1}_{n\times n}+\mathbf{K}_P\boldsymbol{\mathcal{L}}\mathbf{K}_P\right) & \mathbf{0}_{n\times n}\\ \mathbf{0}_{n\times n} & c\left(\mathbf{1}_{n\times n}+\mathbf{K}_Q\boldsymbol{\mathcal{L}}\mathbf{K}_Q\right)\end{bmatrix}.$$

The main objective is to derive conditions guaranteeing that matrix $\boldsymbol{J}$ is Hurwitz, meaning that the real parts of its eigenvalues have all negative signs and, in turn, (27) is stable. Since $\boldsymbol{J}$ consists of block matrices with the bottom right matrix being $\mathbf{0}_{2n\times2n}$, we can use the pertaining quadratic eigenvalue problem to characterize the resulting eigenvalues. The characteristic equation of (27) can thus be calculated through [30]:

$$\det\left(\lambda\boldsymbol{I}_{2n\times2n}-\boldsymbol{J}\right)=\det\left(\boldsymbol{I}_{2n\times2n}\lambda^2+\boldsymbol{J}_{11}\lambda+\boldsymbol{J}_{12}\boldsymbol{J}_{21}\right)=0. \tag{28}$$

Left multiplication of (28) by $\det\left(\boldsymbol{J}_{12}^{-1}\right)$ gives:

$$\det\left(\boldsymbol{J}_{12}^{-1}\lambda^2 + \boldsymbol{H}\lambda + \boldsymbol{J}_{21}\right) = 0, \tag{29}$$

where $\boldsymbol{H} = \boldsymbol{J}_{12}^{-1}\boldsymbol{J}_{11}$.

Theorem 16 of [23] states that if $\boldsymbol{J}_{12}^{-1}$ is positive definite ($\boldsymbol{J}_{12}^{-1} \succ 0$), $\boldsymbol{H}$ can be written as $\boldsymbol{H} = \boldsymbol{F}+\boldsymbol{G}$, where $\boldsymbol{F} \succ 0$ and $\boldsymbol{G}$ skew-symmetric ($\boldsymbol{G} = -\boldsymbol{G}^\intercal$) and $\boldsymbol{J}_{21}$ is positive semi-definite ($\boldsymbol{J}_{21} \succeq 0$), then the real parts of the eigenvalues of $\boldsymbol{J}$ are all non-positive. This result can be interpreted as (27) being marginally stable, as there can also exist zero eigenvalues. Furthermore, if $\boldsymbol{J}_{21} \succ 0$, the eigenvalues of $\boldsymbol{J}$ all have negative real parts and the dynamics of (27) are asymptotically stable. The first condition $\boldsymbol{J}_{12}^{-1} \succ 0$ is already satisfied as $\boldsymbol{J}_{12}$ constitutes a diagonal positive-definite symmetric matrix.

Proposition 1. *Matrix $\boldsymbol{H}$ can be decomposed into a sum of a positive definite matrix and a skew-symmetric matrix, $\boldsymbol{H} = \boldsymbol{F} + \boldsymbol{G}$, where $\boldsymbol{F} \succ 0$ and $\boldsymbol{G} = -\boldsymbol{G}^{\intercal}$.*

Proof: We start the proof by rewriting $\boldsymbol{H}$ as follows:

$$\boldsymbol{H} = \begin{bmatrix} \mathbf{K}_{zd}^{-1}(\boldsymbol{R} + \mathbf{K}_{pd}) & \omega \mathbf{K}_{zd}^{-1}\boldsymbol{L}_{\epsilon} \\ -\omega \mathbf{K}_{zq}^{-1}\boldsymbol{L}_{\epsilon} & \mathbf{K}_{zq}^{-1}(\boldsymbol{R} + \mathbf{K}_{pq}). \end{bmatrix} \tag{30}$$

A necessary condition for Proposition 1 to hold is that the off-diagonal block matrices of $\boldsymbol{H}$ satisfy:

$$\omega \mathbf{K}_{zd}^{-1}\boldsymbol{L}_{\epsilon} = \left(\omega \mathbf{K}_{zq}^{-1}\boldsymbol{L}_{\epsilon}\right)^{\intercal}, \tag{31}$$

or alternatively

$$\mathbf{K}_{zd} = \mathbf{K}_{zq}. \tag{32}$$

This expression states that $k_{zd,i} = k_{zq,i}$, leading to the following sufficient stability criterion:

$$\mathbf{K}_{zd} = \mathbf{K}_{zq} = \mathbf{K}_{z} = \mathrm{diag}(k_{z,1}, \dots, k_{z,n}), \tag{33}$$

where $k_{z,i}$ for $i = 1, 2, \dots, n$, are positive scalars. This stability condition is equivalent to making the i-th VSI d- and q- axis integrator gains equal. This practice is common in power system applications, where a similar settling time of the dq currents is desirable. Nevertheless, due to the structure of $\boldsymbol{J}_{11}$, we deduce the following remark.

Remark 2. *If $\boldsymbol{L}_{\epsilon} = \mathbf{0}_{n\times n}$, then matrix $\boldsymbol{J}_{11}$ is diagonal with all entries positive, thus making $\boldsymbol{J}_{11} \succ 0$. This leads to $\boldsymbol{H} \succ 0$ regardless of the structure of $\mathbf{K}_{zd}$ and $\mathbf{K}_{zq}$. Therefore, when the decoupling process is exact, Proposition 1 holds regardless of (33), for $\boldsymbol{G} = \mathbf{0}_{n\times n}$ and $\boldsymbol{H} = \boldsymbol{F}$.*

Regardless of this remark, we continue the analysis after replacing (33) in (30) and notice that $\boldsymbol{H}$ can be decomposed into the following matrix sum:

$$\boldsymbol{H} = \boldsymbol{F} + \boldsymbol{G}, \tag{34}$$

where

$$\boldsymbol{F} = \begin{bmatrix} \mathbf{K}_{z}^{-1}(\boldsymbol{R} + \mathbf{K}_{pd}) & \mathbf{0}_{n\times n} \\ \mathbf{0}_{n\times n} & \mathbf{K}_{z}^{-1}(\boldsymbol{R} + \mathbf{K}_{pq}) \end{bmatrix},$$

$$\boldsymbol{G} = \begin{bmatrix} \mathbf{0}_{n\times n} & -\omega \mathbf{K}_{z}^{-1}\boldsymbol{L}_{\epsilon} \\ \omega \mathbf{K}_{z}^{-1}\boldsymbol{L}_{\epsilon} & \mathbf{0}_{n\times n} \end{bmatrix}.$$

As $\boldsymbol{F}$ is diagonal with all entries positive, it is also positive definite, while matrix $\boldsymbol{G}$ is skew-symmetric, i.e., $\boldsymbol{G} = -\boldsymbol{G}^{\intercal}$. ■

Proposition 2. *Matrix $\boldsymbol{J}_{21}$ is positive definite ($\boldsymbol{J}_{21} \succ 0$).*

Proof: As $\boldsymbol{J}_{21}$ is block diagonal and composed by symmetric matrices, it becomes apparent that $\boldsymbol{J}_{21} \succ 0$ is equivalent to $\mathbf{1}_{n\times n} + \mathbf{K}_{P}\boldsymbol{\mathcal{L}}\mathbf{K}_{P}, \mathbf{1}_{n\times n} + \mathbf{K}_{Q}\boldsymbol{\mathcal{L}}\mathbf{K}_{Q} \succ 0$, since c is a positive scalar. Therefore, to prove Proposition 2 it is enough to show that the diagonal matrices of $\boldsymbol{J}_{21}$ are positive-definite.

Matrix $\mathbf{1}_{n\times n}$ is rank $\left(\mathbf{1}_{n\times n}\right) = 1$ and contains the zero eigenvalue with multiplicity $n-1$ and the eigenvalue n with multiplicity 1. Matrix $\mathbf{K}_{P}\boldsymbol{\mathcal{L}}\mathbf{K}_{P}$ is congruent to $\boldsymbol{\mathcal{L}}$ due to $\mathbf{K}_{P}$ being symmetric. Invoking Sylvester's law of inertia it becomes apparent that $\mathbf{K}_{P}\boldsymbol{\mathcal{L}}\mathbf{K}_{P}$ and $\boldsymbol{\mathcal{L}}$ share the same index of inertia, that is the triplet vector that describes the number of eigenvalues with positive, negative and zero real part [26]. Accordingly, matrix $\mathbf{K}_P\boldsymbol{\mathcal{L}}\mathbf{K}_P$ has $n-1$ positive eigenvalues and one equal to zero, similarly to $\boldsymbol{\mathcal{L}}$. Furthermore, $\mathbf{K}_P\boldsymbol{\mathcal{L}}\mathbf{K}_P$ is symmetric, since:

$$\left(\mathbf{K}_P\boldsymbol{\mathcal{L}}\mathbf{K}_P\right)^{\intercal} = \mathbf{K}_P^{\intercal}\boldsymbol{\mathcal{L}}^{\intercal}\mathbf{K}_P^{\intercal} = \mathbf{K}_P\boldsymbol{\mathcal{L}}\mathbf{K}_P. \tag{35}$$

Thus, $\mathbf{K}_P\boldsymbol{\mathcal{L}}\mathbf{K}_P \succeq 0$. We recall that the sum of two positive semi-definite matrices results in at least a positive semi-definite matrix, thus making $\mathbf{1}_{n\times n} + \mathbf{K}_P\boldsymbol{\mathcal{L}}\mathbf{K}_P \succeq 0$. In similar fashion, it can be shown that $\mathbf{1}_{n\times n} + \mathbf{K}_Q\boldsymbol{\mathcal{L}}\mathbf{K}_Q \succeq 0$ and therefore $\boldsymbol{J}_{21} \succeq 0$. It is noted that this result, already, validates the stable nature of (27), as according to [23], for $\boldsymbol{J}_{21} \succeq 0$, (27) can be characterized as marginally stable.

Recalling Sylvester's criterion, to show that $\boldsymbol{J}_{21} \succ 0$ it is enough to prove that $\mathbf{1}_{n\times n}+\mathbf{K}_P\boldsymbol{\mathcal{L}}\mathbf{K}_P$ and $\mathbf{1}_{n\times n}+\mathbf{K}_Q\boldsymbol{\mathcal{L}}\mathbf{K}_Q$ are non-singular [26]. In this frame, Lemma 1.2 from [22] is considered, stating that the determinant of a rank-1 update of the Laplacian matrix can be calculated by:

$$\det\left(\boldsymbol{\mathcal{L}} + \boldsymbol{u}\boldsymbol{w}^{\intercal}\right) = \sum u_i \sum w_i \tau, \tag{36}$$

where $\boldsymbol{u} = \left[u_1 \dots u_n\right]^{\intercal}$, $\boldsymbol{w} = \left[w_1 \dots w_n\right]^{\intercal}$ are arbitrary column vectors and $\tau = \left(\lambda_1 \cdot \lambda_2 \cdots \lambda_{n-1}\right)/n$ being the number of spanning trees of $\boldsymbol{\mathcal{L}}$ with $\lambda_1, \dots, \lambda_{n-1}$ being its eigenvalues and n its dimension, respectively.

The proof that $\boldsymbol{J}_{21} \succ 0$ for the trivial case where $\mathbf{K}_P$, $\mathbf{K}_Q$ are equal to the identity matrix is straightforward and summarized in the following remark

Remark 3. *Using (36), and for $\mathbf{K}_P = \mathbf{K}_Q = \boldsymbol{I}_{n\times n}$, $\boldsymbol{u} = \boldsymbol{w} = \mathbf{1}_n$, we deduce that the determinants of matrices $\mathbf{1}_{n\times n} + \mathbf{K}_P\boldsymbol{\mathcal{L}}\mathbf{K}_P$ and $\mathbf{1}_{n\times n} + \mathbf{K}_Q\boldsymbol{\mathcal{L}}\mathbf{K}_Q$ are positive. Consequently, $\boldsymbol{J}_{21} \succ 0$ and Proposition 2 holds.*

An interesting case is when $\mathbf{K}_P$ and $\mathbf{K}_Q$ do not coincide with the identity matrix and are chosen arbitrarily. In this context, it is still possible to prove that the determinants of $\mathbf{1}_{n\times n}+\mathbf{K}_P\boldsymbol{\mathcal{L}}\mathbf{K}_P$ and $\mathbf{1}_{n\times n}+\mathbf{K}_Q\boldsymbol{\mathcal{L}}\mathbf{K}_Q$ are non-zero, regardless of the entries of $\mathbf{K}_P$ and $\mathbf{K}_Q$. The analysis that follows is focused on $\mathbf{1}_{n\times n} + \mathbf{K}_P\boldsymbol{\mathcal{L}}\mathbf{K}_P$, but similar steps can be taken to prove the same properties for $\mathbf{1}_{n\times n} + \mathbf{K}_Q\boldsymbol{\mathcal{L}}\mathbf{K}_Q$. Denoting $g = \sum u_i \sum w_i \tau$, equation (36) is rewritten as:

$$\det\left(\boldsymbol{\mathcal{L}} + \boldsymbol{u}\boldsymbol{w}^{\intercal}\right) = g. \tag{37}$$

We proceed with left and right multiplication of (37) with $\det\left(\mathbf{K}_P\right)$ and due to the determinant multiplication properties:

$$\det\left(\mathbf{K}_P\boldsymbol{\mathcal{L}}\mathbf{K}_P + \mathbf{K}_P\boldsymbol{u}\boldsymbol{w}^{\intercal}\mathbf{K}_P\right) = g\det\left(\mathbf{K}_P\right)^2. \tag{38}$$

Since $\boldsymbol{u}$, $\boldsymbol{w}$ constitute arbitrary column vectors, suppose that they satisfy the following equation:

$$\mathbf{K}_P\boldsymbol{u}\boldsymbol{w}^{\intercal}\mathbf{K}_P = \mathbf{1}_{n\times n}. \tag{39}$$

In this way, (38) is reformed into:

$$\det\left(\mathbf{K}_P\boldsymbol{\mathcal{L}}\mathbf{K}_P + \mathbf{1}_{n\times n}\right) = g\det\left(\mathbf{K}_P\right)^2. \tag{40}$$

To conclude the analysis, it is necessary to show that the imposed transformation of (39) is feasible and secondly, that it does not make $g = 0$. The second condition is very crucial when selecting $\boldsymbol{u}$ and $\boldsymbol{w}$ as g is dependent on the sum of their elements. In this sense, the transformation of (39) is rewritten after multiplying both sides with the non-singular matrix $\mathbf{K}_P^{-1}$:

$$\boldsymbol{u}\boldsymbol{w}^{\intercal} = \mathbf{K}_P^{-1}\mathbf{1}_{n\times n}\mathbf{K}_P^{-1}. \tag{41}$$

Since $\mathbf{K}_P$ is symmetric, all of its powered forms are also symmetric, including the power -1. Therefore, the right hand-side matrix of (41) is congruent to $\mathbf{1}_{n\times n}$ and share the same index of inertia. This is critical for this analysis as the same index of inertia with $\mathbf{1}_{n\times n}$ can be interpreted as being rank-1, since $\mathbf{1}_{n\times n}$ has only 1 non-zero eigenvalue. It is a known fact that through the multiplication of two column vectors it is only possible to produce rank-1 matrices and therefore (41) has at least one solution. What remains is to characterize the nature of $\boldsymbol{u}$, $\boldsymbol{w}$ so as to ensure that $g \neq 0$. As a first step, it is observed that all entries of the matrices comprising the right-hand side of (41) are non-negative

Table 2
LEC controller and system parameters.

Member i	1	2	3	4	5	6	7	8	9	10	11	12	13	14	15	16
r_i [Ω]	0.04	0.07	0.05	0.14	0.07	0.03	0.14	0.15	0.07	0.02	0.04	0.07	0.09	0.04	0.10	0.11
l_i [mH]	1.7	3.0	1.0	2.8	2.9	2.6	1.2	1.5	1.7	2.4	1.2	2.5	1.2	2.3	2.0	2.6
$l_{\epsilon,i}$ [mH]	-0.01	0	-0.04	-0.03	0.03	-0.05	0.04	0.03	0	0.01	-0.03	-0.01	0.05	0.01	0	-0.03
$k_{P,i}$	1	1.7	1.6	1.5	1.3	1.8	.9	.45	.5	1.65	1.55	1.6	1.4	1.5	1.3	1.1
$k_{Q,i}$	1.8	.9	.45	1.3	.5	1.65	1.55	1.3	1	1.7	1.6	1.4	1.6	1.5	1.4	1.5
$k_{pd,i}$	24	21	20	24	23	22	25	23	23	25	24	23	21	21	25	20
$k_{pq,i}$	20	22	21	25	25	24	24	21	20	24	23	22	25	23	23	24
$k_{z,i}$ [$\times 10^{-3}$]	18.8	18.7	17.6	19.2	17.6	17.6	18.8	17.7	19.6	19.6	19.3	17.8	19.2	18.8	20.0	19.1

Table 3
LEC base loads.

Member i	1	2	3	4	5	6	7	8	9	10	11	12	13	14	15	16	17	18	19	20
$P_{l,i}$ [pu]	0.05	0	0	0.1	0.15	0.1	0	0.05	0.1	0	0.05	0.1	0.05	0.1	0.1	0	0.05	0.05	0	0.05
$Q_{l,i}$ [pu]	-0.05	-0.1	-0.2	0	0	-0.1	0.5	0.2	0.3	-0.1	0	0.5	-0.2	-0.3	-0.4	-0.1	-0.05	-0.1	-0.05	-0.1

and since $\mathbf{K}_P^{-1}$ is full rank, the entries of $\mathbf{K}_P^{-1}\mathbf{1}_{n\times n}\mathbf{K}_P^{-1}$ are positive. It is also highlighted that since $\mathbf{K}_P^{-1}$ is symmetric then also $\boldsymbol{u}\boldsymbol{w}^\intercal$ is a symmetric matrix. If we denote $\boldsymbol{B} = \mathbf{K}_P^{-1}\mathbf{1}_{n\times n}\mathbf{K}_P^{-1}$, with $b_{ij} > 0$ being its entries, then (41) can be rewritten as:

$$\begin{bmatrix} u_1 \\ u_2 \\ \vdots \\ u_n \end{bmatrix}\begin{bmatrix} w_1 & w_2 & \cdots & w_n \end{bmatrix} = \begin{bmatrix} b_{11} & b_{12} & \cdots & b_{1n} \\ b_{21} & b_{22} & \cdots & \vdots \\ \vdots & \vdots & \ddots & \vdots \\ b_{n1} & \cdots & \cdots & b_{nn} \end{bmatrix}. \tag{42}$$

Let's consider the first two elements of the first line of $\boldsymbol{B}$:

$$u_1 w_1 = b_{11},\ u_1 w_2 = b_{12}. \tag{43}$$

No elements of $\boldsymbol{u}$, $\boldsymbol{w}$ can be zero as this would result in an element of $\boldsymbol{B}$ being zero, thus contradicting the definition of b_{ij}. As b_{11} and b_{12} are both positive they can be equated through an arbitrary positive scalar, namely d_{11} as $b_{11} = d_{11} b_{12}$. Replacing b_{11} and b_{12} from (41):

$$u_1 w_1 = d_{11} u_1 w_2, \tag{44}$$

which is simplified to:

$$w_1 = d_{11} w_2. \tag{45}$$

Since d_{11} is positive, w_1 and w_2 have to share the same sign. The same properties can be proven for u_1, u_2 by following a similar analysis for the first two elements of the first column of $\boldsymbol{B}$. Furthermore, since $b_{ij} > 0$, the entries of both u_i and w_i must have the same sign. Repeating the same process for the rest of the elements of the first line and first column of $\boldsymbol{B}$ validates that $\boldsymbol{u}$, $\boldsymbol{w}$ have no zero entries and all their elements share identical signs, indicating that $g \neq 0$. Consequently, the determinants of $\mathbf{1}_{n\times n} + \mathbf{K}_P \boldsymbol{\mathcal{L}} \mathbf{K}_P$ and equivalently $\mathbf{1}_{n\times n} + \mathbf{K}_Q \boldsymbol{\mathcal{L}} \mathbf{K}_Q$ are non-zero, verifying Proposition 2 for $\mathbf{K}_P, \mathbf{K}_Q \neq \boldsymbol{I}$. ■

As all conditions of Theorem 16 in [23] are fulfilled, we characterize the stability of (27) through the following corollary.

Corollary 1. *Model (27) is asymptotically stable if (33) is satisfied, regardless of model-parameter uncertainty, including the inductance mismatch captured by $\boldsymbol{L}_\epsilon$. Also, for $\mathbf{K}_P, \mathbf{K}_Q = \boldsymbol{I}$, (27) is asymptotically stable regardless of (33).*

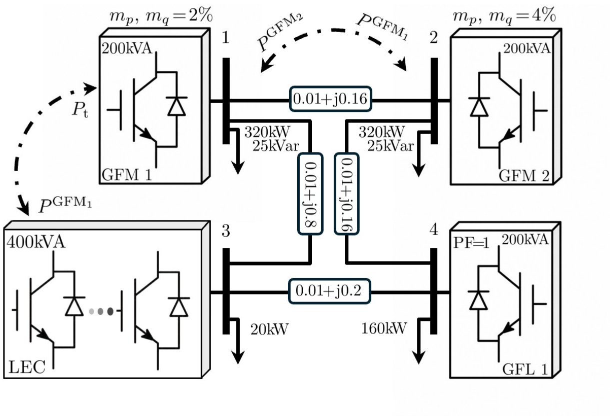

Figure 4: Test network for grid-supporting LEC coordination.

4. Simulation Results

This section presents numerical simulation results that evaluate the performance and stability of the proposed control scheme in two representative test cases. The first test case considers the grid-connected LEC of Fig. 1, where the main grid is modeled as a rigid voltage source with fixed frequency and magnitude. In this setting, the direct power control scheme of (6)–(9) is used to validate the theoretical properties derived in Section 3, namely aggregate active- and reactive-power regulation, proportional power sharing among coordinated members, and robustness against load variations and stochastic power injections from non-coordinated resources. The base demand considered in this case study is given in Table 3. The second test case extends the analysis by integrating the same LEC into the modified test network of [31], as illustrated in Fig. 4. In this configuration, the coordinated members implement the grid-supporting architecture of Fig. 3, where the proposed coordination layer operates together with P–f and Q–v droop control. The droop coefficients are selected as $\boldsymbol{m}_P = 3\mathbf{K}_P\%$ and $\boldsymbol{m}_Q = 2\mathbf{K}_Q\%$. The active power reference P_t^{ref}, which may conventionally be assigned by market participation, is dynamically adjusted by a secondary DAPI controller for frequency restoration [31]. Only the LEC and the grid forming (GFM) inverters participate in the aFRRs, with communication graph $\boldsymbol{\mathcal{L}}_s = [\,2,\ -1,\ -1;\ -1,\ 1,\ 0;\ -1,\ 0,\ 1\,]$ and equal active-power sharing at the secondary-control level. For voltage regulation, the reactive-power reference of the Q–v droop loop, both at the LEC and at each GFM inverter, is adjusted by a local PI controller that drives the corresponding terminal voltage to its nominal value. Bus 4, which hosts a RES-based plant, also implements a GFL scheme, but participates neither in the aFRRs nor in the local voltage-restoration loops, operating instead under constant power-factor mode.

The simulated LEC consists of 20 parallel-connected 20 kVA VSIs at the PCC. In both test cases, only $n = 16$ units participate in the coordination framework, while the remaining $N - n = 4$ units operate under conventional PQ control. The coordinated VSIs communicate with the smart meter and with their two nearest participating community members, producing a communication graph with $n - 1$ edges whose topology is encoded by the Laplacian matrix $\boldsymbol{\mathcal{L}}$. Communication delays are assumed negligible due to the close proximity of the community resources and are therefore not considered. The system and control parameters are provided in Table 2 and satisfy the sufficient stability conditions of Corollary 1; random inductance mismatches between actual and estimated filter values are introduced to assess robustness against parameter uncertainty. The PLLs are configured with a bandwidth of 5 Hz and a damping ratio of $1/\sqrt{2}$. The simulation parameters were selected from the nominal ratings of the considered inverter units, with small perturbations introduced to represent a heterogeneous LEC rather than a set of identical converters. All simulations were performed in Matlab.

In the considered scenario, the active and reactive power outputs of the non-coordinated members are assumed to exhibit a stochastic response (see Fig. 5), modeled as white noise functions. Additionally, the measurements acquired via the smart meter are corrupted with low-level noise to evaluate the controller's response under ambient conditions. The community reference active and reactive powers, $P_{\mathrm{t}}^{\mathrm{ref}}$ and $Q_{\mathrm{t}}^{\mathrm{ref}}$ are both set to zero to avoid any significant power imports/exports and maintain a power neutral operation. The LEC response is illustrated in Figs. 6a-6d. It is evident that the LEC objectives are achieved as the units coordinated by the proposed controller are able to effectively satisfy

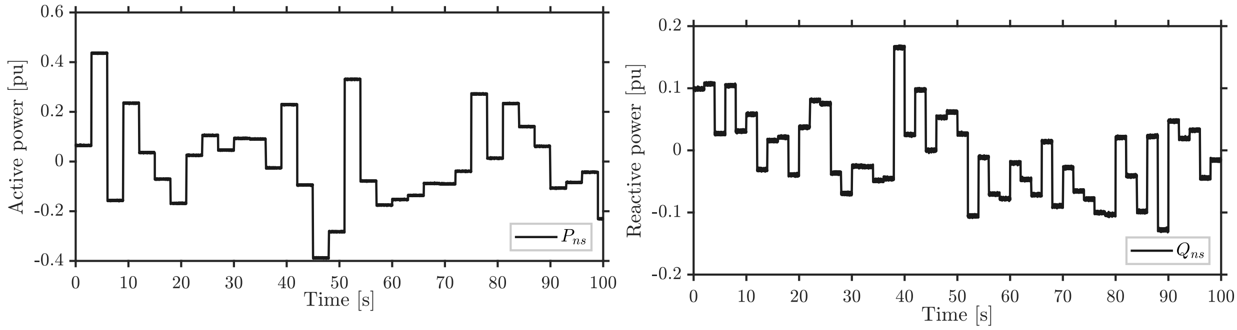

(a) Active power.

(b) Reactive power.

Figure 5: Power output of non-coordinated VSIs.

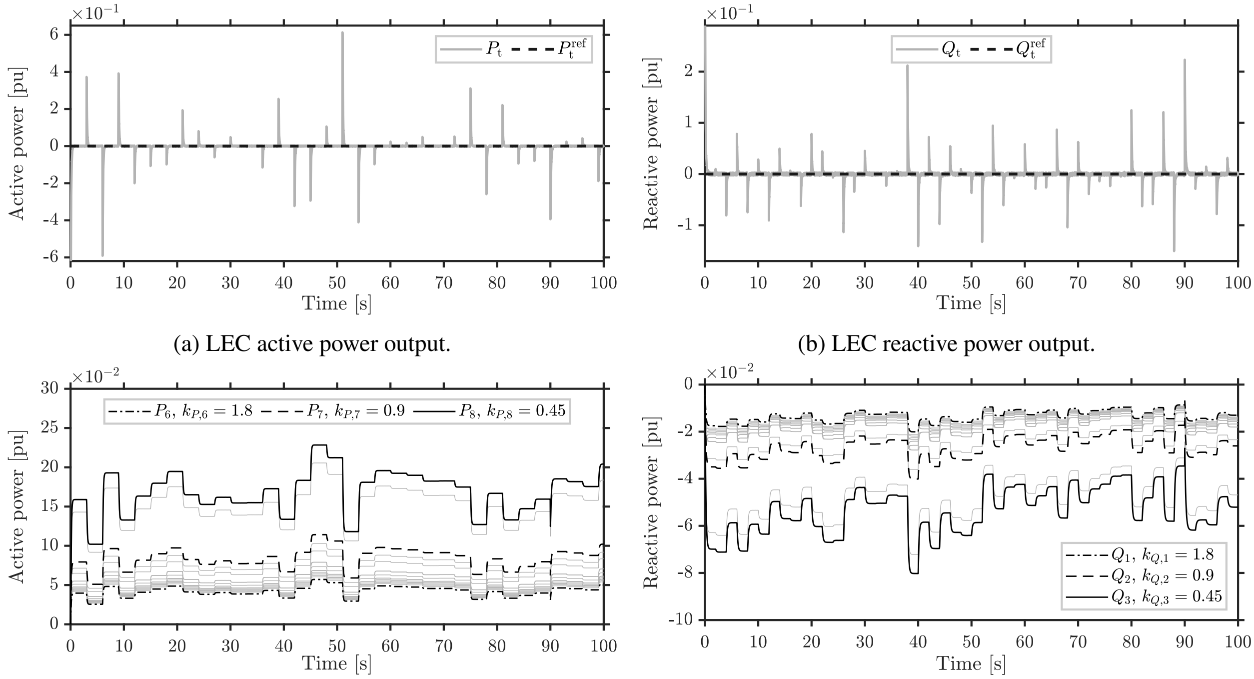

(a) LEC active power output.

(b) LEC reactive power output.

(c) Participating VSIs' active power output.

(d) Participating VSIs' reactive power output.

Figure 6: LEC response under stochastic operation of non-participating VSI.

(4). An interesting occurrence is that the average values of P_{t} and Q_{t} are converging to zero (active and reactive power reference set points), as shown in Figs. 6a and 6b. This is a result induced by the zero mean-value of the white-noise function used to model the stochastic behavior of the non-coordinated units, illustrated in Fig. 5. The effect of the low-power noise originating from the smart meter measurements is subtle and does not impact stability. Also, it is observed from Figs. 6c-6d that despite the rapid variations of the non-coordinated IBRs, the proportional relationship between the active and reactive power outputs of the power-sharing participants is preserved. The settling time of the active and reactive power is approximated at 3 s.

Several disturbances are considered in the second case study to assess the interaction between LEC coordination and grid-supporting operation. At $t = 20$ s, the load at bus 3 is abruptly doubled; at $t = 70$ s, the power of the non-coordinated LEC members is increased by 0.075 pu; at $t = 120$ s, the load at bus 4 is decreased by 20 %; and at $t = 170$ s, the active power of the non-coordinated members is decreased by 0.175 pu. The results are illustrated in Fig. 7. The coordinated LEC units preserve the proportional active- and reactive-power relations imposed by $\mathbf{K}_P$ and $\mathbf{K}_Q$, as shown in Figs. 7c and 7d, despite both network-level disturbances and variations from non-coordinated

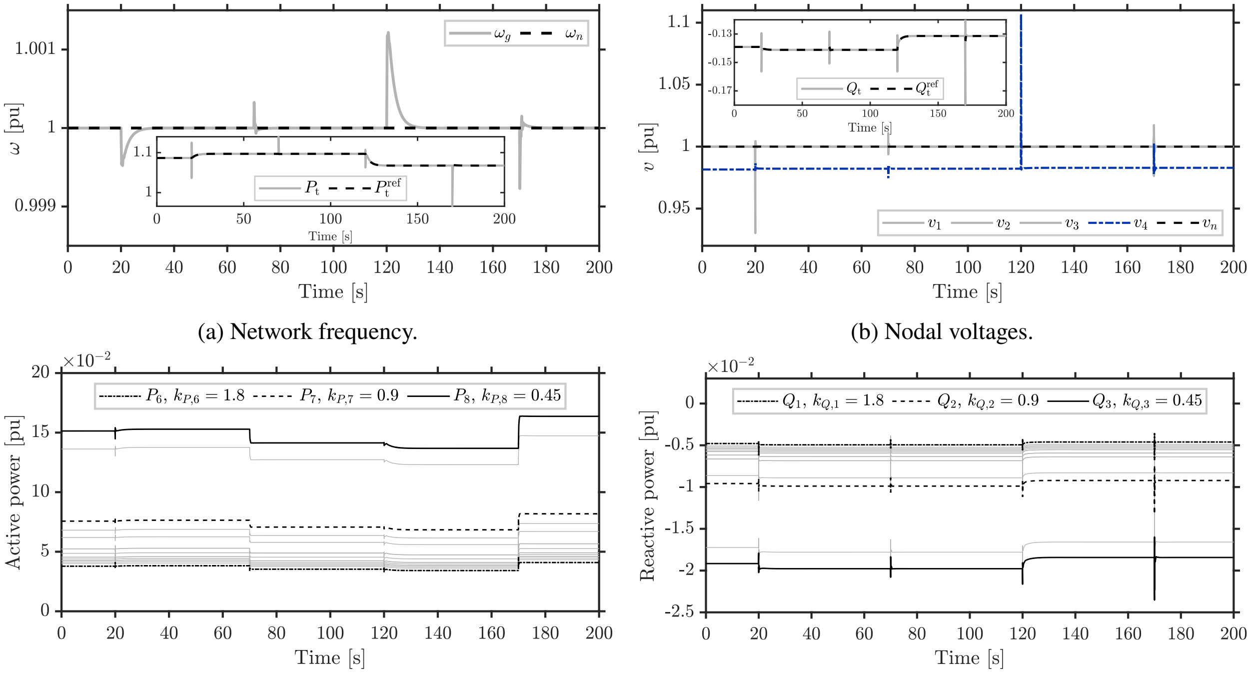

(a) Network frequency.

(b) Nodal voltages.

(c) Participating VSIs' active power output.

(d) Participating VSIs' reactive power output.

Figure 7: Grid-supporting LEC response.

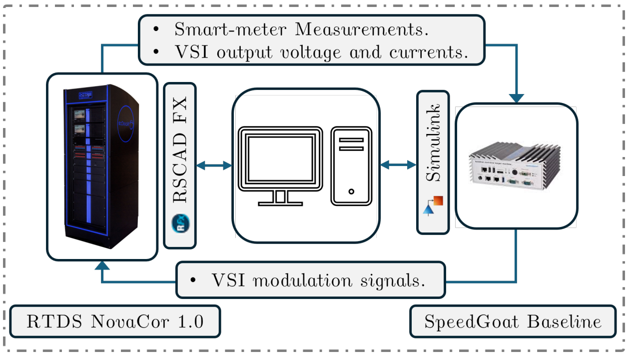

Figure 8: Experimental testbed.

members. The proportional sharing is also maintained even after frequency restoration, as shown in Fig. 7a, where the frequency offset $\omega_n - \omega_g$ is driven to zero without disturbing the prescribed sharing among the coordinated units. This is in contrast to stand-alone primary droop control, where proportional sharing is generally associated with a nonzero steady-state frequency deviation. The aggregate active power of the LEC follows the reference generated by the secondary controller, while the reactive-power response exhibits analogous tracking behavior, as shown in Fig. 7b. Voltage restoration is achieved through the local PI controllers acting on Q_t^{ref} and on the reactive-power references of the GFM implementations. The voltage at bus 4 remains close to its nominal value due to the grid-supporting control loop of the RES-based plant; however, exact restoration is not achieved because this bus does not participate in secondary voltage control.

Table 4
CHIL benchmark parameters.

Member i	1	2	3
r_i [Ω]	0.04	0.07	0.05
l_i [mH]	1.0	3.0	2.0
$k_{P,i}$	1	1	2
$k_{Q,i}$	1	1	2
$k_{pd,i} = k_{pq,i}$	1	1	1
$k_{z,i}$ $\left[\times 10^{-3}\right]$	6.0	6.0	6.0

Table 5
Experimental testbench LEC base loads.

Member i	1	2	3	4
$P_{l,i}$ [pu]	0.4	0.1	0.6	0.4
$Q_{l,i}$ [pu]	-0.05	-0.1	-0.05	0

5. Experimental Results

In this section, we demonstrate the real-world applicability of the proposed LEC coordination scheme through a CHIL testbench. Specifically, a grid-connected LEC is implemented in an RTDS NovaCor 1.0 using the RSCAD graphical environment, according to the setup shown in Fig. 1. The smart meter is realized within RTDS at the PCC terminal, providing aggregated active and reactive power measurements in accordance with Fig. 1. The community consists of four 20 kVA VSIs, three of which are coordinated by the operator to satisfy the community objectives, while the remaining unit operates under PQ control. The control systems of the participating VSIs are implemented in Speedgoat Baseline, which generates SPWM pulses for each individual VSI separately; these pulses are subsequently sent to RTDS, thereby closing the control loop. The controller of the non-coordinated IBR is implemented directly in RTDS. Both RSCAD and Matlab, used respectively to operate the RTDS and program the Speedgoat Baseline, are deployed on a host PC equipped with an Intel Core Ultra 7 255H processor and 16 GB of RAM, connected to both devices via Ethernet. The smart-meter measurements and the current and voltage outputs of the participating units are transmitted from RTDS to the Speedgoat Baseline via copper cables, while the modulation pulses are routed back to RTDS through the same interface. The switching frequency of the SPWM is set to 8 kHz and the sampling rate to 10 kHz. An illustration of the experimental testbench is depicted in Fig. 8, while the controller and system parameters are listed in Tables 4 and 5, respectively, and were selected following the same procedure as in the simulation studies. The PLL parameters are identical to those of the previous section.

The considered LEC is tested through different disturbances, to ensure that the community coordination scheme can accommodate abnormal operating conditions. These include active and reactive power set point changes, changes in the power output of the non power-sharing unit, load variations, as well as a voltage fault. Specifically, in this scenario we consider that $P_{\mathrm{t}}^{\mathrm{ref}}$ is set to 0.2 pu at $t = 0$ s, then at $t = 20$ s it is increased to 2 pu, subsequently at $t = 50$ s it is changed to -1 pu, while at $t = 80$ s it is restored to 1 pu. On the other hand, $Q_{\mathrm{t}}^{\mathrm{ref}}$ is set to zero for the whole duration of the simulation, maintaining unity power factor. Additionally, at $t = 30$ s the non-coordinated units increase their active and reactive power injection from 0 to 2 pu and 0.5 pu, respectively. These converters stop the active and reactive power injection at $t = 70$ s. Additionally, at $t = 55$ s $P_{l,1}$ is abruptly increased by 0.5 pu. Finally, at $t = 90$ s the grid voltage is reduced from 1 pu to 0.8 pu.

The experimental results are presented in Fig. 9. It can be observed from Fig. 9a that the LEC output tracks effectively the reference signal despite the ongoing disturbances. Fig. 9c illustrates the active power of the coordinated members. Remarkably, regardless of the behavior of the non-coordinated units, the LEC members achieve the power quota of the community and maintain the intended proportional active power relation, i.e., $k_{P,1}P_1 = k_{P,2}P_2 = k_{P,3}P_3$ or equivalently $P_1 = P_2 = 2P_3$. Similar conclusions can be derived from the reactive power output depicted in Fig. 9d, i.e., $k_{Q,1}Q_1 = k_{Q,2}Q_2 = k_{Q,3}Q_3$ or equivalently $Q_1 = Q_2 = 2Q_3$. The controlled VSIs maintain their stability even during the abrupt PCC voltage sag, validating the theoretical analysis conducted in the previous section. The

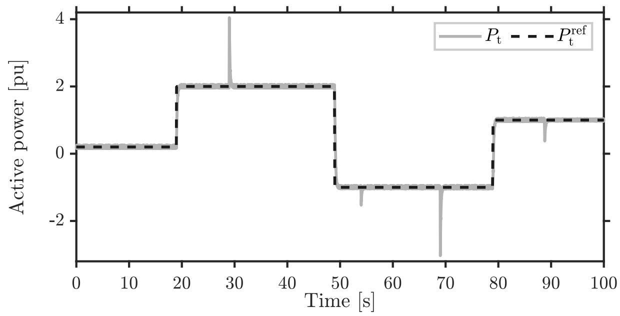

(a) LEC active power output.

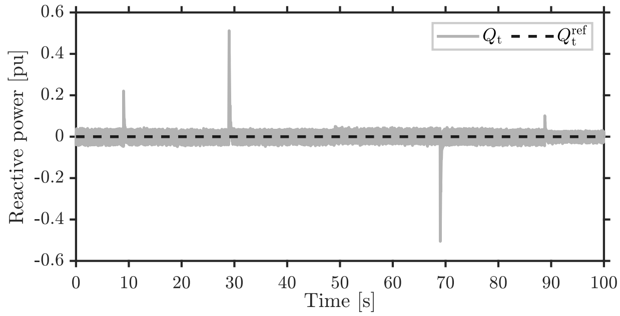

(b) LEC reactive power output.

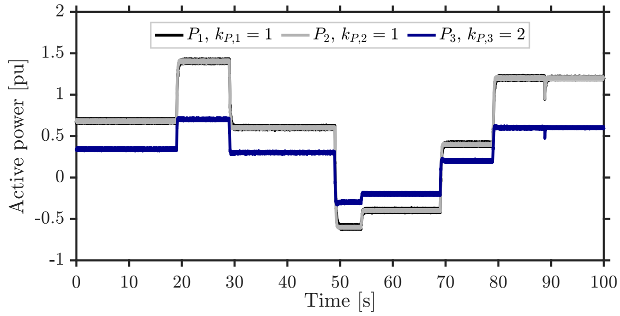

(c) Active power output of participating VSIs.

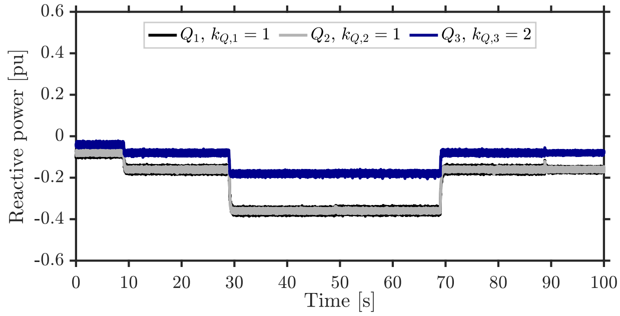

(d) Reactive power output of participating VSIs.

Figure 9: Experimental results of a grid-connected LEC obtained via CHIL.

convergence rate of the LEC relies on the gains of the matrices $\mathbf{K}_{\text{pd}}$, $\mathbf{K}_{\text{pq}}$, $\mathbf{K}_{\text{zd}}$, $\mathbf{K}_{\text{zq}}$ as well as the power sharing coefficient matrices, $\mathbf{K}_{\text{P}}$ and $\mathbf{K}_{\text{Q}}$. Finally, the settling time of the coordinated VSIs is approximately 1 s.

6. Conclusion

A power-coordination scheme is proposed in this paper to regulate clustered DERs within a LEC setting. The scheme regulates the aggregated power output of the LEC while maintaining a proportional relationship between the power outputs of the coordinated members. In this way, it enables real-time coordination of market-participating LECs in accordance with their cleared bids and market obligations, supporting existing tertiary optimizers in avoiding the balancing penalties caused by volatile load and generation. The modularity of the controller allows its integration into existing hierarchical control schemes, enabling market-compliant coordination while the LECs simultaneously provide grid-supporting services. Finally, extensive simulation and experimental scenarios validated the stability and satisfactory performance of the LEC coordination controller and its grid-supporting extensions under ambient and fault conditions.

CRediT authorship contribution statement

Zaint A. Alexakis: Conceptualization, Data curation, Formal analysis, Investigation, Methodology, Resources, Validation, Visualization, Writing – original draft, Writing – review & editing. **Panos C. Papageorgiou:** Conceptualization, Formal analysis, Investigation, Validation, Writing – original draft, Writing – review & editing. **Antonio T. Alexandridis:** Formal analysis, Methodology, Supervision, Writing – original draft, Writing – review & editing. **Georgios Tzounas:** Conceptualization, Formal analysis, Investigation, Methodology, Supervision, Validation, Visualization, Writing – original draft, Writing – review & editing. **Charalambos Konstantinou:** Conceptualization, Formal analysis, Funding acquisition, Investigation, Methodology, Project administration, Supervision, Validation, Writing – original draft, Writing – review & editing.

References

[1] Afshari, A., Davari, M., Karrari, M., Gao, W., Blaabjerg, F., 2024. A Multivariable, Adaptive, Robust, Primary Control Enforcing Predetermined Dynamics of Interest in Islanded Microgrids Based on Grid-Forming Inverter-Based Resources. IEEE Transactions on Automation Science and Engineering 21, 2494–2506. doi:10.1109/TASE.2023.3262852.

[2] Afzali, S., Parsa Moghaddam, M., Sheikh-El-Eslami, M.K., Zamani, R., 2025. A flexibility-oriented bidding strategy for virtual power plants incorporating local energy communities: A bi-level stochastic-robust methodology. Applied Energy 399, 126355. URL: https://www.sciencedirect.com/science/article/pii/S0306261925010852, doi:https://doi.org/10.1016/j.apenergy.2025.126355.

[3] Alexakis, Z.A., Alexandridis, A.T., Papageorgiou, P.C., Konstantopoulos, G.C., 2024. Design of a bandwidth limiting pll for grid-tied inverters with guaranteed stability. IEEE Transactions on Sustainable Energy , 1–11doi:10.1109/TSTE.2024.3483988.

[4] Alexandridis, A.T., 2020. Studying state convergence of input-to-state stable systems with applications to power system analysis. Energies 13. doi:10.3390/en13010092.

[5] Araujo, L.S., Callegari, J.M.S., Cardoso Filho, B.J., Brandao, D.I., 2024. Heterogeneous microgrids: Centralized control strategy with distributed grid-forming converters. International Journal of Electrical Power & Energy Systems 158, 109950. URL: https://www.sciencedirect.com/science/article/pii/S0142061524001716, doi:https://doi.org/10.1016/j.ijepes.2024.109950.

[6] Asimakopoulou, G.E., Hatziargyriou, N.D., 2018. Evaluation of economic benefits of DER aggregation. IEEE Transactions on Sustainable Energy 9, 499–510. doi:10.1109/TSTE.2017.2743349.

[7] Bao, P., Wang, Y., Jiang, X., Wang, Y., Wang, C., 2025. A Statistical-Based Approach for Decentralized Demand Response Toward Primary Frequency Support: A Case Study of Large-Scale 5G Base Stations With Adaptive Droop Control. IEEE Transactions on Smart Grid 16, 2208–2221. doi:10.1109/TSG.2025.3535729.

[8] Bidram, A., Davoudi, A., 2012. Hierarchical structure of microgrids control system. IEEE Transactions on Smart Grid 3, 1963–1976. doi:10.1109/TSG.2012.2197425.

[9] Chandorkar, M., Divan, D., Adapa, R., 1993. Control of parallel connected inverters in standalone ac supply systems. IEEE Transactions on Industry Applications 29, 136–143. doi:10.1109/28.195899.

[10] Chang, S., Wang, C., Luo, X., Guan, X., 2024. Distributed predefined-time secondary control under directed networks for dc microgrids. Applied Energy 374, 123993. URL: https://www.sciencedirect.com/science/article/pii/S030626192401376X, doi:https://doi.org/10.1016/j.apenergy.2024.123993.

[11] Chang, W., Yang, Q., 2026. Coordinated Electricity and Carbon Emission Management for Active Power Distribution Systems Considering Local Carbon Trading. Protection and Control of Modern Power Systems 11, 175–188. doi:10.23919/PCMP.2024.000393.

[12] Chen, S., Liu, W., Guo, Z., Zhang, S., Yang, Z., Chung, C.Y., 2025. Aggregating large-scale residential users for regulation reserve provision: Truthful combinatorial auction based approach. IEEE Transactions on Sustainable Energy 16, 686–699. doi:10.1109/TSTE.2024.3479451.

[13] Correa-Florez, C.A., Michiorri, A., Kariniotakis, G., 2020. Optimal participation of residential aggregators in energy and local flexibility markets. IEEE Transactions on Smart Grid 11, 1644–1656. doi:10.1109/TSG.2019.2941687.

[14] Cui, S., Wang, Y.W., Li, C., Xiao, J.W., 2020. Prosumer community: A risk aversion energy sharing model. IEEE Transactions on Sustainable Energy 11, 828–838. doi:10.1109/TSTE.2019.2909301.

[15] De Blasis, R., Pacelli, G., Vergine, S., 2026. Investment valuation of photovoltaic and energy storage systems for diverse energy communities: A real option approach. Applied Energy 404, 127185. URL: https://www.sciencedirect.com/science/article/pii/S0306261925019154, doi:https://doi.org/10.1016/j.apenergy.2025.127185.

[16] Dos Santos, L.E., Flores Huaman, J., Carlos Ugaz Peña, J., Duarte Queiroz, E., Dotta, D., 2025. A Data-Driven Centralized Secondary Control Design Methodology for Microgrids. IEEE Transactions on Smart Grid 16, 2738–2751. doi:10.1109/TSG.2025.3558108.

[17] Eghtedarpour, N., Farjah, E., 2014. Power control and management in a hybrid ac/dc microgrid. IEEE Transactions on Smart Grid 5, 1494–1505. doi:10.1109/TSG.2013.2294275.

[18] Eskandari, M., Li, L., Moradi, M.H., Siano, P., Blaabjerg, F., 2019. Active power sharing and frequency restoration in an autonomous networked microgrid. IEEE Transactions on Power Systems 34, 4706–4717. doi:10.1109/TPWRS.2019.2923797.

[19] Fan, B., Li, Q., Wang, W., Yao, G., Ma, H., Zeng, X., Guerrero, J.M., 2022. A novel droop control strategy of reactive power sharing based on adaptive virtual impedance in microgrids. IEEE Transactions on Industrial Electronics 69, 11335–11347. doi:10.1109/TIE.2021.3123660.

[20] García-Cerezo, Á., Bonilla, D., Baringo, L., García-González, J., 2026. A Stochastic Adaptive Robust Optimization Approach to Build Day-Ahead Bidding Curves for an EV Aggregator. IEEE Transactions on Industry Applications 62, 244–256. doi:10.1109/TIA.2025.3587193.

[21] Haben, S., Singleton, C., Grindrod, P., 2016. Analysis and clustering of residential customers energy behavioral demand using smart meter data. IEEE Transactions on Smart Grid 7, 136–144. doi:10.1109/TSG.2015.2409786.

[22] Klee, S., Stamps, M.T., 2021. Eigenvalues of graph Laplacians via rank-one perturbations. The Quarterly Journal of Mathematics 73, 609–616. doi:10.1093/qmath/haab045, arXiv:https://academic.oup.com/qjmath/article-pdf/73/2/609/44082127/haab045.pdf.

[23] Lancaster, P., 2013. Stability of linear gyroscopic systems: A review. Linear Algebra and its Applications 439, 686–706. doi:https://doi.org/10.1016/j.laa.2012.12.026. Special Issue in Honor of Harm Bart.

[24] Liu, J., Miura, Y., Bevrani, H., Ise, T., 2017. Enhanced virtual synchronous generator control for parallel inverters in microgrids. IEEE Transactions on Smart Grid 8, 2268–2277. doi:10.1109/TSG.2016.2521405.

[25] Liu, Z., Xing, L., Fang, J., Shu, Z., Su, H., 2025. Distributed Secondary Control for DC Microgrids With Near-Infinite Constant Power Load Accommodation. IEEE Transactions on Smart Grid 16, 4451–4462. doi:10.1109/TSG.2025.3605924.

[26] Meyer, C., 2000. Matrix Analysis and Applied Linear Algebra. Other Titles in Applied Mathematics, Society for Industrial and Applied Mathematics.

[27] Ning, B., Han, Q.L., Ding, L., 2021. Distributed finite-time secondary frequency and voltage control for islanded microgrids with communication delays and switching topologies. IEEE Transactions on Cybernetics 51, 3988–3999. doi:10.1109/TCYB.2020.3003690.

[28] Palizban, O., Kauhaniemi, K., 2015. Hierarchical control structure in microgrids with distributed generation: Island and grid-connected mode. Renewable and Sustainable Energy Reviews 44, 797–813. doi:https://doi.org/10.1016/j.rser.2015.01.008.

[29] Qiu, H., Gu, W., Xu, Y., Zhao, B., 2019. Multi-time-scale rolling optimal dispatch for ac/dc hybrid microgrids with day-ahead distributionally robust scheduling. IEEE Transactions on Sustainable Energy 10, 1653–1663. doi:10.1109/TSTE.2018.2868548.

[30] Silvester, J.R., 2000. Determinants of block matrices. The Mathematical Gazette 84, 460–467.

[31] Simpson-Porco, J.W., Shafiee, Q., Dörfler, F., Vasquez, J.C., Guerrero, J.M., Bullo, F., 2015. Secondary frequency and voltage control of islanded microgrids via distributed averaging. IEEE Transactions on Industrial Electronics 62, 7025–7038. doi:10.1109/TIE.2015.2436879.

[32] Singh, C., Sreekumar, S., Malakar, T., 2026. Balancing markets and imbalance forecasting: A pathway towards net zero grids. Applied Energy 402, 126976. URL: https://www.sciencedirect.com/science/article/pii/S0306261925017064, doi:https://doi.org/10.1016/j.apenergy.2025.126976.

[33] Su, J., Zhang, H., Liu, H., Liu, D., 2025. Lyapunov-based distributed secondary frequency and voltage control for distributed energy resources in islanded microgrids with expected dynamic performance improvement. Applied Energy 377, 124539. URL: https://www.sciencedirect.com/science/article/pii/S0306261924019226, doi:https://doi.org/10.1016/j.apenergy.2024.124539.

[34] Wanapinit, N., Thomsen, J., 2026. Benefits and allocation principles of sector-coupled energy communities. Applied Energy 410, 127497. URL: https://www.sciencedirect.com/science/article/pii/S0306261926001492, doi:https://doi.org/10.1016/j.apenergy.2026.127497.

[35] Wang, B., Zhou, P., Zhang, C., Chen, X., Dong, Z.Y., 2026. Coordinated Interaction Between EV Charging Stations and Distribution Network via Stepwise Droop Control with SoC Interval Management. IEEE Transactions on Sustainable Energy , 1–13doi:10.1109/TSTE.2026.3679752.

[36] Xia, Z., Abu Qahouq, J.A., 2021. State-of-charge balancing of lithium-ion batteries with state-of-health awareness capability. IEEE Transactions on Industry Applications 57, 673–684. doi:10.1109/TIA.2020.3029755.

[37] Yan, D., Ma, C., Chen, Y., 2023. Distributed coordination of charging stations considering aggregate ev power flexibility. IEEE Transactions on Sustainable Energy 14, 356–370. doi:10.1109/TSTE.2022.3213173.

[38] Yu, T., Islam, M.M., Zhou, L., Wang, Z., La Scala, M., Wang, J., Guan, X., Yao, G., 2025. Hierarchical multi-time-scale energy management system for secure and economic operation of islanded microgrids with gfm/gfl control. Applied Energy 397, 126359. URL: https://www.sciencedirect.com/science/article/pii/S030626192501089X, doi:https://doi.org/10.1016/j.apenergy.2025.126359.

[39] Zhang, L., Capuder, T., Mancarella, P., 2016. Unified unit commitment formulation and fast multi-service lp model for flexibility evaluation in sustainable power systems. IEEE Transactions on Sustainable Energy 7, 658–671. doi:10.1109/TSTE.2015.2497411.

[40] Zhong, Q.C., 2013. Robust droop controller for accurate proportional load sharing among inverters operated in parallel. IEEE Transactions on Industrial Electronics 60, 1281–1290. doi:10.1109/TIE.2011.2146221.